

Article

Binary Encounter Electrons in Fast Dressed-Ion–H₂ Collisions: Distorted Wave Theories and Experiment

Nicolás J. Esponda ¹, Stefanos Nanos ², Michele A. Quinto ¹, Theo J. M. Zouros ³, Roberto D. Rivarola ^{1,4}, Emmanouil P. Benis ^{2,*} and Juan M. Monti ^{1,4,*}

¹ Instituto de Física Rosario (CONICET-UNR), Bv 27 de Febrero 210 bis, Rosario 2000, Argentina

² Department of Physics, University of Ioannina, GR-45110 Ioannina, Greece

³ Department of Physics, University of Crete, GR-70013 Heraklion, Greece

⁴ Laboratorio de Colisiones Atómicas, FCEIA, IFIR, Universidad Nacional de Rosario, Avenida Pellegrini 250, Rosario 2000, Argentina

* Correspondence: mbenis@uoi.gr (E.P.B.); monti@ifir-conicet.gov.ar (J.M.M.)

Abstract: We report measurements of double differential cross section for zero-degree binary encounter electrons emitted in collisions of 4.9 MeV and 13 MeV B^{(2–5)+} ions with H₂ targets. The corresponding calculations based on continuum distorted-wave (CDW) theories are critically compared to the measurements. CDW in its post form exhibits a very good agreement with the measurements in all cases. The CDW theories utilized along with the well-known eikonal-initial-state (CDW-EIS) approximation are also examined and their results are compared to both the measurements and the CDW calculations. In particular, CDW-EIS using a recently proposed dynamic effective charge for the final channel projectile distortion exhibits a substantial improvement in comparison with an effective net-charge approximation.

Keywords: ion-atom collisions; binary encounter electrons; distorted wave theories



Citation: Esponda, N.J.; Nanos, S.; Quinto, M.A.; Zouros, T.J.M.; Rivarola, R.D.; Benis, E.P.; Monti, J.M. Binary Encounter Electrons in Fast Dressed-Ion–H₂ Collisions: Distorted Wave Theories and Experiment. *Atoms* **2023**, *11*, 17. <https://doi.org/10.3390/atoms11020017>

Academic Editor: Károly Tökési

Received: 12 December 2022

Revised: 14 January 2023

Accepted: 16 January 2023

Published: 20 January 2023



Copyright: © 2023 by the authors. Licensee MDPI, Basel, Switzerland. This article is an open access article distributed under the terms and conditions of the Creative Commons Attribution (CC BY) license (<https://creativecommons.org/licenses/by/4.0/>).

1. Introduction

For high velocity, $v > Z_p$, bare-ion projectiles impinging on atomic targets, the binary encounter electron (BEE) emission spectra are an important benchmark where classical [1] and quantum theories are expected to converge. BEE are target electrons ionized through direct, hard collisions, give rise to a peak structure whose maximum position can be classically predicted from energy and momentum conservation laws, obtaining the well-known $k = 2v \cos \theta$ result, where k and θ are the momentum and emission angle of the ejected electron, respectively. The BEE peak is characteristic of the double differential cross section (DDCS) electron spectra, the width of which is attributed to the initial momentum distribution of the electron in the target atom, and while the peak is not seen in the SDCS spectra, since the BEE maximum continuously varies in energy with respect to the electron emission angle, it plays a major role in the determination of the SDCS profile [2].

The BEE peak results from the elastic scattering between the projectile and a target electron. Thus, it is expected that the BEE peak maximum increases with increasing projectile charge state. In particular, a Z_p^2 scaling law is classically expected for the bare projectile DDCS, in accordance with the Rutherford scattering [3]. However, it has been evidenced [4–8] that for dressed projectiles a higher BEE peak was observed at zero degrees compared to the corresponding BEE peak of bare ions, contrary to the classical picture prediction [9]. This enhancement was theoretically explained as a consequence of the non-Coulombic interaction between dressed projectiles and the target electron [4,5].

Another characteristic feature of the BEE peak in collisions of dressed projectiles is the formation of oscillatory structures at certain ejection angles, which was experimentally exposed by several groups in the early 1990s [10–12]. The structured BEE peak can be viewed within the framework of a free-electron model, where, for a certain projectile charge

state, target electrons are elastically scattered from a non-Coulombic field. In the quantum mechanical wave picture, these oscillations can be attributed to diffraction effects, which can only be observed under certain conditions [2].

The continuum distorted-wave (CDW) framework was extended for partially dressed ions by Monti et al. in [13,14], where not only the q dependence of the peak magnitude was reproduced for O^{q+} and F^{q+} projectiles colliding with He targets, but also a double-peak structure on the BEE peak for A^{11+} and U^{21+} projectiles was explained as a quantum interference between the transition amplitudes related to the Coulombic and non-Coulombic projectile potential. In Ref [14], the CDW-EIS results could not account for the BEE peak q -dependence. In this work, we show how the projectile's effective dynamic charge presented in [15] makes a significant change in those calculations. Current calculations also include the projectile ionization, which was not considered in [14], despite its negligible contribution at zero-degree BEE. The results of the CDW and CDW-EIS theories are directly compared to a new set of zero-degree DDCS BEE measurements for 4.9 and 13 MeV $B^{(2-5)+} + H_2$ collisions.

2. Experiment

The experimental data were obtained using the zero-degree Auger projectile spectroscopy (ZAPS) setup which has been described in detail elsewhere [16–18]. The cornerstone of the ZAPS setup is the electron spectrograph which consists of an electrostatic hemispherical deflector analyzer (HDA) equipped with a four-element injection lens and a two-dimensional position sensitive detector (PSD). The projectile travels through a doubly differentially pumped gas cell, where it interacts with the gas target, and continues through the spectrograph to be collected in a Faraday cup for normalization purposes. The electrons emitted at zero degrees with respect to the projectile direction are focused by the spectrograph entry lens, energetically analyzed by the HDA and imaged onto the PSD [19,20]. The ZAPS setup is currently located at the NCSR “Demokritos” 5.5 MV Tandem Accelerator Laboratory [21]; however, the reported measurements were taken when the setup was operating at the J.R. Macdonald Laboratory.

The measured electron DDCS is determined according to the following formula [22]:

$$DDCS_j \equiv \frac{d^2\sigma_j}{d\Omega dE_j} = \frac{N_j^e}{N_I L_{eff} n \Delta\Omega \Delta E_j T \eta} \quad (1)$$

where N_j^e is the number of electrons detected in channel j , L_{eff} the effective length of the target gas cell, N_I the number of ions collected in the Faraday cup, n the target gas density, $\Delta\Omega$ the solid angle determined by the entry aperture of the lens and the distance of the center of the target gas cell from it, ΔE_j the energy step per channel in the spectrum and T the transmission of the three electroformed meshes of the analyzer (90% transmission each). The overall efficiency factor, η , is determined in collisions of bare projectiles with H_2 targets. There, the BEE electron yield, determined from Equation (1) except for the overall efficiency η , is normalized to the corresponding theoretical BEE DDCS, calculated using the classical Rutherford scattering within the impulse approximation [22]. Thus, for the reported measurements, an overall detection efficiency of $\eta = (35 \pm 4)\%$ was determined.

Since a ZAPS spectrum can be recorded simultaneously in one energy window covering an energy range of about 20% of the analyzer tuning energy, several overlapped energy windows, obtained at the appropriate tuning energies, were pieced together to obtain the BEE peaks [23]. For each energy window, a subtraction of the background signal, corresponding to a measurement without target gas, was performed. The resulting spectrum was energy calibrated according to known energy vs. channel calibration formulae, and the DDCS were then obtained according to Equation (1). Single-collision conditions were ensured by properly adjusting the target gas pressure. An overall absolute uncertainty of about 20% is inherent in all of our measurements.

3. Theory

Let us study the single ionization reaction in a collision system between an atomic or molecular target and a projectile, which may also carry its own bounded electrons, using continuum distorted-wave theories. This is a difficult multielectronic problem that can be rather simplified under the independent electron approximation. In this way, we assume that the projectile electrons and those of the target, which are not emitted, remain frozen in their own initial state. These electrons are called the *passive* ones, whereas the one being ejected from the target is referred to as the *active* electron. Furthermore, under the impact parameter approximation, we can ignore the interaction between the projectile and the target nucleus. Therefore, the one-electron Hamiltonian in the laboratory reference frame is given by (atomic units used throughout this section unless otherwise stated):

$$H_{el} = -\frac{1}{2}\nabla_r^2 + V_T(\mathbf{x}) + V_P(\mathbf{s}), \tag{2}$$

where r is a generic label for the spatial coordinates, for which we make the usual non-orthogonal choice of \mathbf{x} and \mathbf{s} as the position of the active electron relative to the target and projectile nucleus, respectively. In addition, $V_T(\mathbf{x})$ is the target potential, while $V_P(\mathbf{s})$ is the interaction between the active electron and the screened projectile. According to the work presented in [24–26], we may approximate V_P with a two-parameter Green-Sellin-Zachor [27–29] potential of the form

$$V_P(\mathbf{s}) = -\frac{q}{s} - \frac{1}{s}(Z_P - q)[H(e^{s/d} - 1) + 1]^{-1}, \tag{3}$$

where H and d are parameters that depend on the projectile nuclear charge, Z_P , and its number of electrons N [14,29]. Note that the first term in Equation (3) represents the asymptotic Coulomb interaction, with $q = Z_P - N$, while the second term describes the screened short-range interaction.

Treating the projectile-active-electron interaction as a perturbation, the initial and final distorted wave functions are proposed to be

$$\chi_i^+(\mathbf{r}, t) = \Phi_i(\mathbf{x}, t)\mathcal{L}_i^+(\mathbf{s}) \tag{4a}$$

$$\chi_f^-(\mathbf{r}, t) = \Phi_f(\mathbf{x}, t)\mathcal{L}_f^-(\mathbf{s}), \tag{4b}$$

where the initial target bound state $\Phi_i(\mathbf{x}, t) = \phi_i(\mathbf{x}) \exp(-i\varepsilon_i t)$ and its final continuum state $\Phi_f(\mathbf{x}, t) = \phi_f(\mathbf{x}) \exp(-i\varepsilon_f t)$ are multiplied by a projectile continuum distortion factor $\mathcal{L}_i^+(\mathbf{s})$ and $\mathcal{L}_f^-(\mathbf{s})$, respectively. The target final state is taken as an hydrogenic continuum wavefunction with the Belkić target effective charge prescription [30], while the target bound state is described by Roothaan-Hartree-Fock wave functions decomposed in terms of atomic Slater-type orbitals given by [31]. In the case of a molecular orbital (MO), it can also be approximated by the linear combinations of its atomic compound orbitals (LCAOs), and then, neglecting the overlap between the atomic orbitals (CNDO approximation), the final MO DDCS corresponds to the sum of the atomic orbitals DDCS weighted by the electronic population [32]. In this framework, the H₂ molecule ionization DDCS will be twice the hydrogen atom DDCS.

The transition amplitude can be defined in its *prior*, $a_{if}^-(\rho)$, or *post*, $a_{if}^+(\rho)$, forms depending on whether the operators act over the initial or final wavefunction (or channel), namely

$$a_{if}^-(\rho) = -i \int_{-\infty}^{+\infty} \left\langle \chi_f^- \left| \left(H_{el} - i \frac{\partial}{\partial t} \right) \right| \chi_i^+ \right\rangle dt \tag{5a}$$

$$a_{if}^+(\rho) = -i \int_{-\infty}^{+\infty} \left\langle \chi_f^- \left| \left(H_{el} - i \frac{\partial}{\partial t} \right)^\dagger \right| \chi_i^+ \right\rangle dt. \tag{5b}$$

Considering the distortion factors in Equation (4), the choice of their functional form results in different CDW approximations. Two of them, the CDW post and the CDW-EIS prior, will be briefly presented below.

3.1. CDW Post Theory

Choosing a hydrogenic continuum factor for the projectile distortion in the initial and final channel corresponds to the CDW approximation. Here, the distortions are

$$\mathcal{L}_i^+(\mathbf{s}) = N^*(\nu) {}_1F_1[-i\nu, 1, -i(\nu\mathbf{s} + \mathbf{v} \cdot \mathbf{s})] \quad (6a)$$

$$\mathcal{L}_f^-(\mathbf{s}) = N^*(\xi) {}_1F_1[-i\xi, 1, -i(p\mathbf{s} + \mathbf{p} \cdot \mathbf{s})], \quad (6b)$$

where ${}_1F_1$ is the confluent hypergeometric function, $N(a) = \Gamma(1 - ia) \exp(\pi a/2)$ its normalization factor, \mathbf{v} the projectile velocity, $\mathbf{p} = \mathbf{k} - \mathbf{v}$ the momentum of the ejected electron in the projectile frame, \mathbf{k} the ejected electron momentum in the target reference frame, $\nu = Z_P^{\text{eff}}/k$ and $\xi = Z_P^{\text{eff}}/p$ for some effective projectile nuclear charge Z_P^{eff} , for now taken to be the asymptotic net charge, i.e., $Z_P^{\text{eff}} = q$.

Since the prior version of the transition amplitude of the CDW theory is known to have intrinsic divergences near the BEE peak [33], the post version of Equation (5b) is utilised throughout the CDW calculations instead. In order to use a hydrogenic continuum with an effective charge Z_T^{eff} as the final state ϕ_f in the target-electron subsystem, we rewrite its potential as

$$V_T(\mathbf{x}) = -\frac{Z_T^{\text{eff}}}{x} - \frac{(Z_T - Z_T^{\text{eff}})}{x} + V_{ap}(\mathbf{x}), \quad (7)$$

where $V_{ap}(\mathbf{x})$ is the interaction between the active electron and the target's passive ones [14]. Then, the second and third terms of Equation (7) are left unsolved by Φ_f . It is usual to discard these terms from the transition amplitude because their inclusion, in what is called the *complete post* CDW theory, may make the mentioned divergences reappear. A detailed study of such divergences has been performed by Monti et al. in [34], where a so-called *complete hybrid post* CDW theory has also been reported. In the present work, since we are approximating the H₂ molecule ionization DDCS as twice the corresponding H atom ionization DDCS, both the initial bound and final continuum target states are exact solutions of the one-electron Hamiltonian. Consequently, there is no difference between *post* and *prior* versions of CDW [35]. Moreover, whenever we are addressing hydrogenic targets with no passive electrons, the V_{ap} residual term is null.

3.2. CDW-EIS Prior Theory

In the case where instead of the hydrogenic continuum factor of Equation (6a) we take its asymptotic limit ($\mathbf{v} \cdot \mathbf{s} \rightarrow \infty$) given by

$$\mathcal{L}_i^+(\mathbf{s}) = \exp[-i\nu \ln(\nu\mathbf{s} + \mathbf{v} \cdot \mathbf{s})], \quad (8)$$

we obtain the CDW eikonal-initial-state (CDW-EIS) approximation. In this framework, there are no divergences in the transition amplitude, and thus its *prior* version (Equation (5a)) is utilized since it makes it possible to fully include the target potential by the initial bound state ϕ_i . As a result, CDW-EIS in its prior version can be extended more easily to a wide variety of atomic and molecular targets.

Regarding the final channel distortion, we take it as in Equation (6b). However, the projectile effective charge may be taken as the dynamic one presented by Esponda et al. in [15]. This dynamic effective charge is defined as a function of the momentum transfer \mathbf{K} through the projectile's form factor $F(\mathbf{K})$, namely

$$Z_P^{\text{eff}}(K) = Z_P - F(\mathbf{K}), \quad (9)$$

where, for a projectile remaining in its ground state $\phi_{P_i}(\mathbf{r}_1, \mathbf{r}_2, \dots, \mathbf{r}_N)$ throughout the collision,

$$F(\mathbf{K}) = \left\langle \phi_{P_i} \left| \sum_{j=1}^N e^{i\mathbf{K} \cdot \mathbf{r}_j} \right| \phi_{P_i} \right\rangle. \quad (10)$$

Through this definition, it can be seen that the dynamic charge can have values ranging from $Z_P^{\text{eff}}(K) = Z_P - N$ when $K \rightarrow 0$ to $Z_P^{\text{eff}}(K) = Z_P$ as $K \rightarrow \infty$. Therefore, by the use of this effective charge, we introduce a dynamic screening for the projectile due to its bounded electrons. In contrast, in the initial channel we will preserve the usual asymptotic net charge q for the incoming projectile distortion so as to satisfy the boundary conditions. Let us refer to the CDW-EIS calculations where an asymptotic net charge q is used in both channels as “ $\nu_0 \zeta_0$ ”, and in the case where the dynamic effective charge of Equation (9) is applied only in the final channel distortion as “ $\nu_0 \zeta_K$ ”.

4. Results and Discussion

In this section, we present our experimental and theoretical DDCS results on BEE electrons, ejected at zero degrees in the laboratory rest frame, from collisions of dressed projectiles with gas targets. Specifically, we measured DDCS of BEE peaks for the collision systems of $B^{(2-5)+}$ with H_2 targets in order to have additional testing ground for comparison of the various CDW theories that best treat the binary collisions. Although BEE data are available in the literature and have been used for testing CDW theories [15], to the best of our knowledge, systematic BEE data for boron projectiles are scarce. Thus, we obtained DDCS for BEE peaks for bare, H-like, He-like and Li-like boron projectiles. The low atomic number ($Z_P = 5$) value of boron as well as the relatively lower collision energies challenge perturbation theories such as CDW, and thus offer more stringent tests.

In Figure 1a we present the experimental DDCS electron spectra along with the results from the CDW theories examined in this work, for the collisions of 4.9 MeV $B^{(2-5)+} + H_2$. Only statistical error bars, included within the data points symbol, are shown in the measurements. In addition, an absolute overall uncertainty of about 15%, primarily due to the uncertainty of the overall detection efficiency η , is estimated for all the measurements. The CDW theories in use inherently include the projectile ionization, although it has a negligible effect on the BEE peak, as shown in Appendix B. For the bare B^{5+} projectiles, it is evident that both CDW and CDW-EIS theories give results with negligible differences and in very good agreement with the measurements. This is expected since for energetic head-on electron elastic scattering from bare ions quantum mechanical results are expected to converge to the classical ones. This is the reason for using the Rutherford scattering within the impulse approximation for the absolute normalization of the experimental BEE DDCS, a fact that is justified by the current CDW results.

For the dressed projectiles, $B^{(2-4)+}$, CDW theory (Section 3.1) with asymptotic projectile charge values for both initial and final channels shows an excellent agreement with the measurements at the high energy wing of the BEE peak. CDW-EIS ($\nu_0 \zeta_0$) that uses an asymptotic charge for both the initial and final channels exhibits a large deviation from CDW and measurements, that increases by decreasing the projectile charge state. Moreover, CDW-EIS ($\nu_0 \zeta_0$) fails to reproduce the DDCS enhancement of the BEE peak with the decrease in the projectile charge state. On the contrary, CDW-EIS ($\nu_0 \zeta_K$) that uses an effective dynamic charge for the final channel projectile distortion reproduces to some extent the BEE peak magnitude, although not as accurately as the CDW. In Figure 1a, it can be seen that the deviations of CDW-EIS ($\nu_0 \zeta_K$) from CDW post are also more pronounced with decreasing projectile net charge.

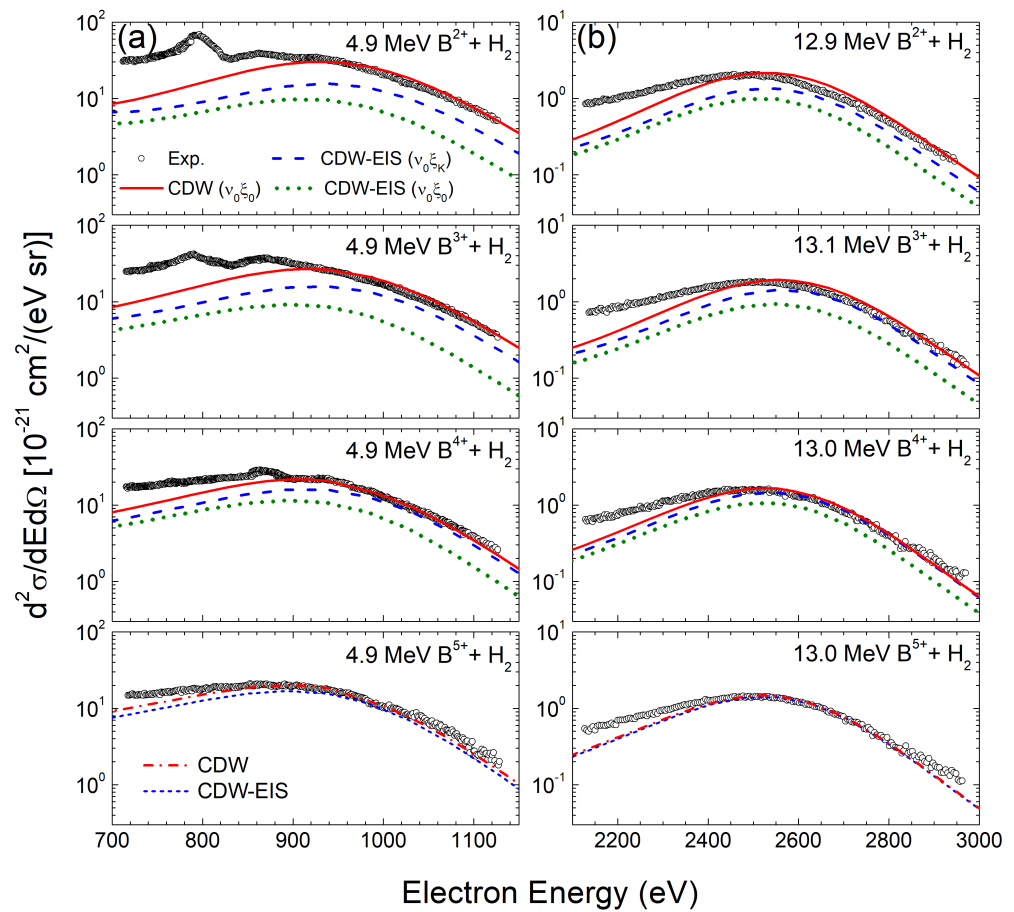


Figure 1. (a) DDCS for zero-degree electron emission angle in collisions of 4.9 MeV $B^{(2-5)+} + H_2$. Experiment: black open circles (statistical error bars are within the symbol). Theory: red lines, CDW (post form) for non-bare ions where an asymptotic charge is used for both the initial and final channels (noted as $\nu_0 \xi_0$); blue dashed line: CDW-EIS (prior form) for non-bare ions where a dynamic charge is applied to the final channel projectile distortion, while an asymptotic charge is used for the initial channel (noted as $\nu_0 \xi_K$); green dotted line: CDW-EIS (prior form) for non-bare ions where the asymptotic charge is used for both the initial and final channels (noted as $\nu_0 \xi_0$); red dash-dotted line: CDW for bare ions; blue short-dashed line: CDW-EIS for bare ions. (b) Same as in (a), but for collisions of 13 MeV $B^{(2-5)+} + H_2$.

On the other hand, the low-energy wing of the BEE peak is underestimated by the three CDW theories. The main reason for such a discrepancy probably lies in the description of the DDCS resulting from the molecular H_2 target as twice the corresponding atomic H DDCS. Even though it may still be a good approximation for the BEE spectrum at higher energies or for estimating H_2 singly differential and total cross sections, using the H atomic orbital is evidently not so accurate for describing the electronic initial momentum distribution (Compton profile) of the H_2 molecular orbital when calculating DDCSs. In Figure 2, we show a CDW calculation for 4.9 MeV B^{5+} and B^{2+} projectiles using an approximate molecular orbital from [36]. As can be seen for B^{5+} , a major improvement in the BEE peak shape is achieved with a more realistic description of the initial bound state. For the case of dressed boron projectiles, it is worth mentioning that the peaks that appear superimposed on the low-energy wing of the BEE peaks correspond to the formation of KLn ($n \geq 2$) Auger states. These states are populated primarily by the processes of transfer-excitation (TE) [37] for the B^{4+} and B^{3+} projectiles, and electron-nucleus excitation (enE) and electron-electron excitation (eeE) [38] for the B^{2+} projectiles which, however, are not described by our CDW models.

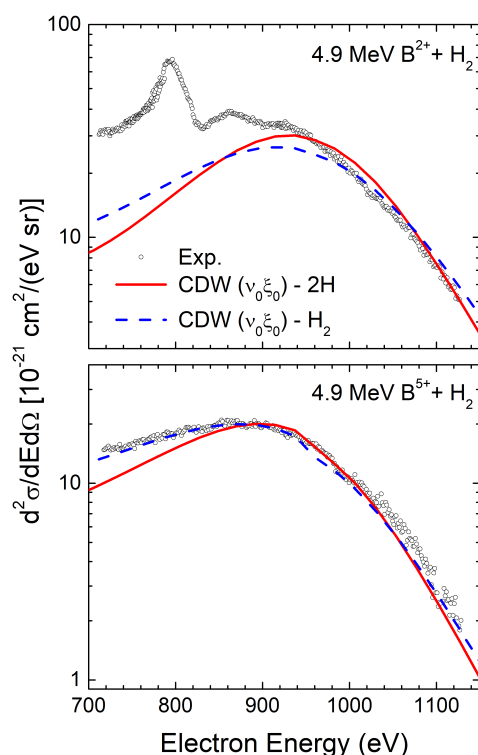


Figure 2. DDCS for zero-degree electron emission angle in collisions of 4.9 MeV $B^{2+} + H_2$ (top) and 4.9 MeV $B^{5+} + H_2$ (bottom). Grey open circles: Experiment. Red solid lines: CDW post with hydrogen atom initial bound state (multiplied by two to account for H_2). Blue dashed line: CDW post with single-term modified-basis H_2 bound state.

To further explore the behavior of the CDW theories, we included a systematic study of the BEE peaks at higher collision energies. In Figure 1b, we present the experimental DDCS electron spectra along with the results from the three CDW theories examined here, for collisions of 13 MeV $B^{(2-5)+} + H_2$. At these higher energies, the CDW and CDW-EIS ($\nu_0 \xi_K$) theories are in much better agreement than in the case of 4.9 MeV collision energy, for a given charge state q . In particular, up to two bounded electrons, B^{3+} , CDW-EIS ($\nu_0 \xi_K$) gives almost the same results as CDW, while CDW-EIS ($\nu_0 \xi_0$) still fails to follow the other CDW theories results after a first bounded electron is considered in the projectile. The deviations of CDW-EIS from CDW are in general smaller in 13 MeV than in 4.9 MeV because as the projectile velocity increases, the eikonal approximation of Equation (8) becomes a better description for the projectile initial channel distortion, as evident by the CDW initial channel distortion of Equation (6a) which tends to Equation (8) as the velocity increases. Nevertheless, the BEE is characterized by short range projectile-target-electron interactions (small s), so better results are still obtained with CDW because the hypergeometric function (Equation (6a)) of the initial channel is a good approximation for all the $\mathbf{v} \cdot \mathbf{s}$ domain (see Appendix A). Comparing CDW-EIS ($\nu_0 \xi_K$) with CDW-EIS ($\nu_0 \xi_0$) results, we can state that the better agreement of CDW-EIS ($\nu_0 \xi_K$) with experimental data for $B^{(3,4)+}$ dressed projectiles is due to the use of the effective dynamic charge in the final channel distortion. The lack of a good initial distortion may be compensated by the interaction with a less screened projectile in the final channel for the high momentum transfers involved in BEE.

A quantitative outcome of such studies, with special interest to experimentalists, is the determination of the so-called BEE enhancement factors, obtained as the ratio of the BEE peak maxima of the dressed projectiles to the corresponding BEE peak maximum of the bare projectiles [9]. In Figure 3a,b, we show the experimental and theoretical BEE enhancement factors as a function of the projectile charge state, q , for the 4.9 MeV and 13 MeV collision energies corresponding to the data of Figure 1. The experimental results show a monotonic increase in the BEE enhancement factor with decreasing q , in accordance

with the results of similar studies reported in the literature [4–9]. The results of the CDW theory reproduce this behavior, exhibiting a very good agreement with the experimental results for the 4.9 MeV collision energy and an excellent agreement with the experimental results for the 13 MeV collision energy. However, both CDW-EIS theories do not reproduce this behavior. CDW-EIS ($\nu_0\zeta_K$) exhibits a rather constant BEE enhancement factor, while CDW-EIS ($\nu_0\zeta_0$) shows a decrease in the BEE enhancement factor with decreasing projectile charge state. However, as can be inferred from Figure 3c, a smaller deviation is evident with increasing collision energy. Thus, as stated above, the inherent BEE short-range interactions are not accurately described by the eikonal phase in the CDW-EIS approximations and thus, even though they reproduce the BEE peak characteristics to some extent, they fail to determine the BEE enhancement factors.

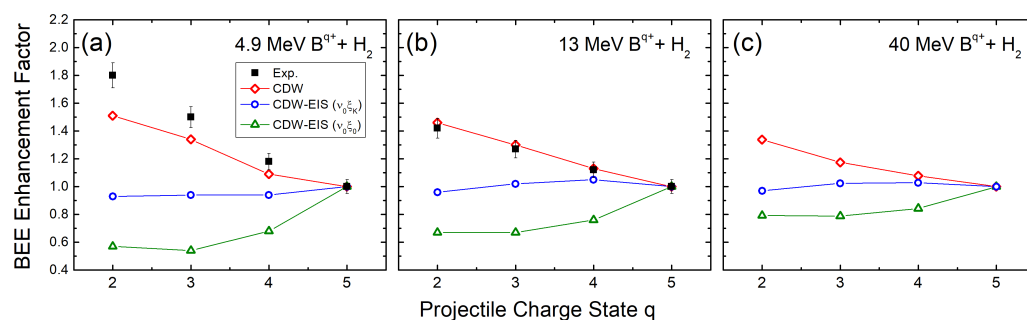


Figure 3. BEE enhancement factors as a function of the projectile charge state for the collision system of $B^{(2-4)+} + H_2$ for the collision energies of (a) 4.9, (b) 13 and (c) 40 MeV. Black filled squares: Experiment. Red open diamonds: CDW. Blue open circles: CDW-EIS ($\nu_0\zeta_K$). Green open triangles: CDW-EIS ($\nu_0\zeta_0$). The lines are drawn to guide the eye.

BEE enhancement factors of dressed projectiles can be used to obtain the absolute normalization of experimental electron yield spectra, thus resulting in DDCSs. The use of bare ions, where a simple Rutherford scattering model can be applied for absolute normalization of the electron yield spectra, would require additional experiments with low beam currents, as usually delivered in this case by tandem Van de Graaff accelerators. Instead, the option of absolutely normalizing the electron yield spectra, by measuring BEE peaks obtained from the dressed projectiles used in each experiment, is favored. In this case, the BEE result of the Rutherford scattering model is simply multiplied with the BEE enhancement factor, obtained from theory, and the measured electron yield spectra are normalized to this result.

In Figure 4, we show our BEE results from the three CDW theories in comparison to the BEE experimental results, reported in [8], for the collision system of 30 MeV $O^{(5-8)+} + He$. The use of He atoms in this collision system allows for a good-quality initial bound-state description, by the use of Roothan-Hartree-Fock wavefunctions from [31]. In general, the behaviors observed in Figure 1 are followed for this system. The CDW results are in very good agreement with the BEE measurements for the high energy wing of the BEE peak, while the agreement is much improved for the lower BEE wing, compared to the collisions of boron ions with molecular H_2 targets. This is due to the more accurate description of the electron initial state in the atomic He target. In addition, CDW-EIS prior ($\nu_0\zeta_0$) exhibits a large deviation both from CDW theory and measurements, while CDW-EIS prior ($\nu_0\zeta_K$) resides in between the CDW and the CDW-EIS prior ($\nu_0\zeta_0$) results. Finally, in Figure 5, we present the BEE enhancement factors obtained experimentally and from the CDW theories. The behavior is similar to that of the the BEE enhancement factors obtained for boron.

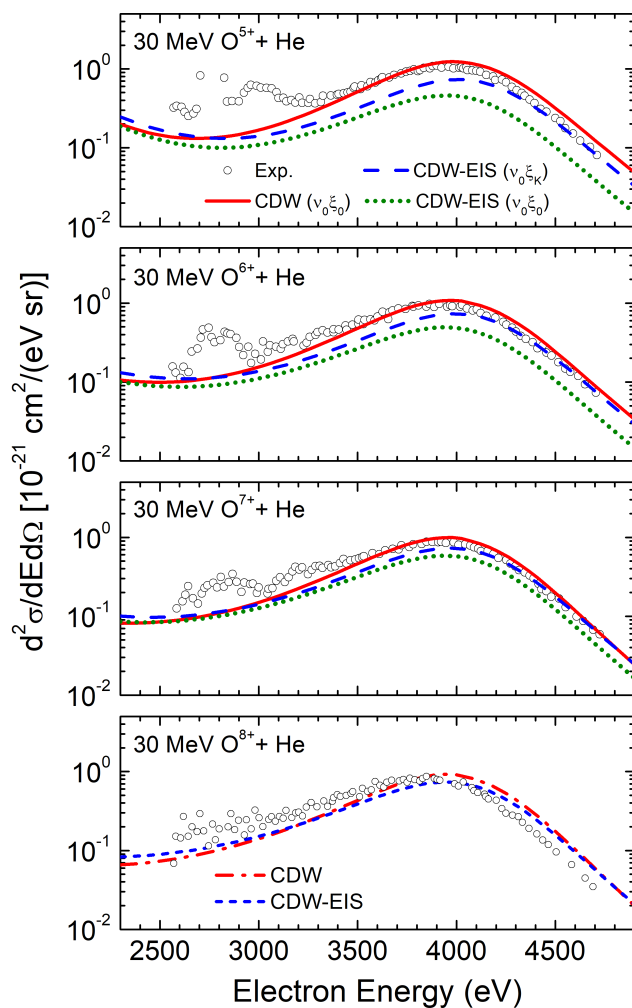


Figure 4. Same as in Figure 1, but for the collision system of 30 MeV $O^{(5-8)+} + He$. Experimental data from Ref. [8].

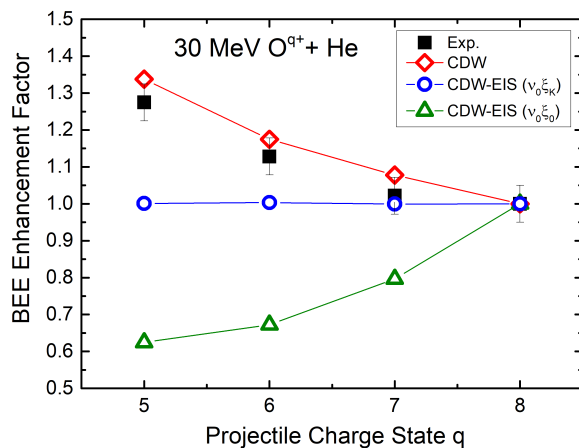


Figure 5. Same as in Figure 3, but for the collision system of 30 MeV $O^{(5-8)+} + He$, corresponding to the data presented in Figure 4.

5. Conclusions

We have performed a systematic study of the zero-degree BEE DDCS as a function of the charge state of bare and dressed boron projectiles, $B^{(2-5)+}$, colliding with H_2 targets at 4.9 MeV and 13 MeV collision energies. Corresponding BEE DDCS results from CDW and CDW-EIS theories are compared to the measurements. The CDW calculations

exhibit an overall very good agreement with the measurements, especially when accurate molecular-type initial state H₂ wavefunctions are considered. This is attributed to the better description of the close encounter region due to the hydrogenic-continuum initial distortion. CDW-EIS, using an asymptotic charge for both the initial and final channel projectile distortion, fails to accurately reproduce the magnitude of the BEE peak. CDW-EIS using a dynamic charge for the final channel projectile distortion and an asymptotic charge for the initial channel shows a good agreement both with the measurements and CDW for H-like boron ions, but substantially deviates for boron ions dressed with more than one electron. In addition, BEE enhancement factors were also obtained. Finally, our study includes similar results for the collision system of 30 MeV O^{(5–8)+} + He, where the use of more accurate initial state atomic wavefunctions resulted in a better agreement for the CDW theory to the measurements for the low-energy wing of the BEE peak.

Author Contributions: Conceptualization, E.P.B. and J.M.M.; methodology, E.P.B., S.N., N.J.E. and J.M.M.; software, N.J.E., M.A.Q. and J.M.M.; validation, R.D.R. and T.J.M.Z.; formal analysis, N.J.E., M.A.Q. and S.N.; investigation, E.P.B., N.J.E., M.A.Q. and J.M.M.; resources, E.P.B. and J.M.M.; data curation, E.P.B. and J.M.M.; writing—original draft preparation, J.M.M., S.N. and E.P.B.; writing—review and editing, J.M.M., E.P.B., T.J.M.Z. and R.D.R.; visualization, E.P.B.; supervision, E.P.B. and J.M.M.; project administration, E.P.B.; funding acquisition, E.P.B. and J.M.M. All authors have read and agreed to the published version of the manuscript.

Funding: This research received no external funding.

Data Availability Statement: The data that support the findings of this study are available from the corresponding authors upon reasonable request.

Acknowledgments: The theoretical results presented in this work have been obtained by using the facilities of the CCT-Rosario Computational Center, member of the High Performance Computing National System (SNCAD, MincyT-Argentina).

Conflicts of Interest: The authors declare no conflict of interest.

Appendix A. Remarks about the Prior and Post Transition Amplitudes

It is important to emphasize the fact that when the target is a hydrogenic atom and the projectile is a fully-stripped ion, then post and prior versions of the transition amplitude do not imply any difference because both the target initial and final wavefunctions are exact [35]. Comparing CDW post and CDW-EIS prior transition amplitudes for the cited system, we obtain the perturbative potentials, after using Equations (6b) and (8), respectively, as

$$W_f^- \chi_f^- = \Phi_f(\mathbf{x}, t) \left[\nabla_{\mathbf{x}} \ln \phi_f(\mathbf{x}) \cdot \nabla_{\mathbf{s}} \mathcal{L}_f^-(\mathbf{s}) \right] \quad (\text{A1a})$$

$$W_i^+ \chi_i^+ = \Phi_i(\mathbf{x}, t) \left[\frac{1}{2} \nabla_{\mathbf{s}}^2 \mathcal{L}_i^+(\mathbf{s}) + \nabla_{\mathbf{x}} \ln \phi_i(\mathbf{x}) \cdot \nabla_{\mathbf{s}} \mathcal{L}_i^+(\mathbf{s}) \right]. \quad (\text{A1b})$$

However, by taking the limit $\mathbf{v} \cdot \mathbf{s} \rightarrow \infty$, Equation (A1b) results in the CDW prior form of the perturbative potential

$$W_i^+ \chi_i^+ = \Phi_i(\mathbf{x}, t) \left[\nabla_{\mathbf{x}} \ln \phi_i(\mathbf{x}) \cdot \nabla_{\mathbf{s}} \mathcal{L}_i^+(\mathbf{s}) \right], \quad (\text{A2})$$

which is equivalent to the CDW post potential, Equation (A1a), since $\mathcal{L}_i^+(\mathbf{s})$ and $\mathcal{L}_f^-(\mathbf{s})$ (exact) have analogous asymptotic behavior, and the target states are exact. Therefore, since we are treating the H₂ molecule ionization DDCS as twice the corresponding DDCS for an H atom, we expect the CDW and CDW-EIS theories to give the same results with bare projectiles at high collision energies (when $Z_p/v < 1$).

Finally, let us address dressed ions impinging on an H target. In Equation (3), we stated that the projectile potential can be written as the sum of (Coulombic) long-range and (non-Coulombic) short-range terms. This will split the transition amplitude into two terms,

one related to the long-range interaction and the other to the short-range interaction. For the long-range interaction, the above post-prior asymptotic equivalence applies, but for the short-range interaction it is different. The Fourier transform of the short-range transition amplitude for either CDW or CDW-EIS [14] is

$$F^{sr}(\mathbf{K}) = \left[\frac{-1}{(2\pi)^{3/2}} \int d\mathbf{x} e^{-i\mathbf{K}\cdot\mathbf{x}} \phi_f^*(\mathbf{x}) \phi_i(\mathbf{x}) \right] \left[\frac{(Z_P - q)}{(2\pi)^{3/2}} \int d\mathbf{s} e^{i\mathbf{K}\cdot\mathbf{s}} \mathcal{L}_f^{-*}(\mathbf{s}) \frac{\Omega(s)}{s} \mathcal{L}_i^+(\mathbf{s}) \right] \quad (\text{A3})$$

where $\Omega(s)$ is the GSZ screening function of Equation (3), namely

$$\Omega(s) = [\text{H}(e^{s/d} - 1) + 1]^{-1}. \quad (\text{A4})$$

The screening function vanishes outside a few atomic radii, and thus the integral over s will only make a significant contribution within a close-encounter domain, i.e., at short distances s . Here, the limit $\mathbf{v} \cdot \mathbf{s} \rightarrow \infty$ is challenged and the eikonal approximation of CDW-EIS (Equation (8)) may differ from the exact hydrogenic continuum (Equation (6a)). This may make CDW-EIS “ $\nu_0 \zeta_0$ ” approximation to be not as good as CDW for BEE calculations; however, it is interesting to study the effect that a projectile dynamic effective charge could have on the CDW-EIS “ $\nu_0 \zeta_K$ ” theory.

Appendix B. Target and Projectile Ionization Contributions

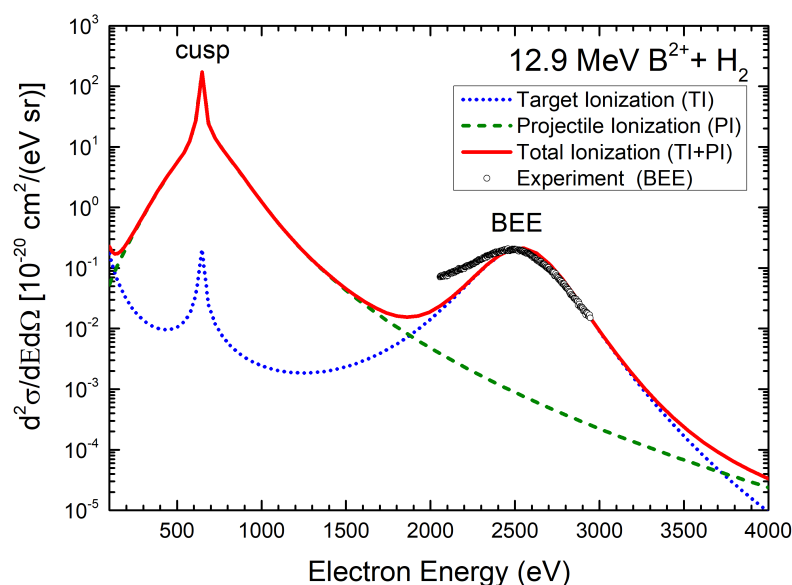


Figure A1. CDW calculations of zero-degree electron spectra for the collision system of 12.9 MeV $\text{B}^{2+} + \text{H}_2$, showing the contributions of target and projectile electron emission in the BEE and cusp energy areas. Blue dotted line: Target ionization. Green dashed line: Projectile ionization. Red solid line: The sum of both target and projectile ionization. Open circles: Experiment. It is clearly seen that projectile ionization, although it is the main contribution for the cusp electrons, for the BEE electrons it is negligible.

References

1. Rutherford, E. The scattering of α and β particles by matter and the structure of the atom. *Lond. Edinb. Dublin Philos. Mag. J. Sci.* **1911**, *21*, 669–688.
2. Stolterfoht, N.; DuBois, R.; Rivarola, R. *Electron Emission in Heavy Ion-Atom Collisions*; Springer Series on Atomic, Optical, and Plasma Physics; Springer: Berlin/Heidelberg, Germany, 1997.
3. Lee, D.H.; Richard, P.; Zouros, T.J.M.; Sanders, J.M.; Shinpaugh, J.L.; Hidmi, H. Binary encounter electrons observed at zero degrees in collisions of 1-2 MeV/amu H^+ , C^{6+} , N^{7+} , O^{8+} and F^{9+} . *Phys. Rev. A* **1990**, *41*, 4816. [[CrossRef](#)] [[PubMed](#)]
4. Reinhold, C.O.; Schultz, D.R.; Olson, R.E. Theoretical description of the binary peak in clothed ion-atom collisions. *J. Phys. B At. Mol. Phys.* **1990**, *23*, L591–L596. [[CrossRef](#)]

5. Schultz, D.R.; Olson, R.E. Binary peak enhancement and structure in partially stripped ion-atom collisions. *J. Phys. B At. Mol. Phys.* **1991**, *24*, 3409–3432. [[CrossRef](#)]
6. Hidmi, H.I.; Richard, P.; Sanders, J.M.; Schöne, H.; Giese, J.P.; Lee, D.H.; Zouros, T.J.M.; Varghese, S.L. Charge-state dependence of binary-encounter-electron cross sections and peak energies. *Phys. Rev. A* **1993**, *48*, 4421–4428. [[CrossRef](#)] [[PubMed](#)]
7. Posthumus, J.H.; Christensen, B.; Glargaard, N.; Madsen, J.N.; Andersen, L.H.; Hvelplund, P.; Grabbe, S.R.; Bhalla, C.P. The enhancement of the binary encounter peak for $q=1$ to Z in collisions of fast C^{q+} and O^{q+} on H_2 . *J. Phys. B At. Mol. Phys.* **1994**, *27*, L97–L102. [[CrossRef](#)]
8. Zouros, T.J.M.; Wong, K.L.; Grabbe, S.; Hidmi, H.I.; Richard, P.; Montenegro, E.C.; Sanders, J.M.; Liao, C.; Hagmann, S.; Bhalla, C.P. 0° binary encounter electron production in 30-MeV $O^{q+}+H_2$, He, O_2 , Ne, and Ar collisions. *Phys. Rev. A* **1996**, *53*, 2272–2280. [[CrossRef](#)]
9. Richard, P.; Lee, D.H.; Zouros, T.J.M.; Sanders, J.M.; Shinpaugh, J.L. Anomalous q dependence of 0° binary encounter electron production in energetic collisions of F^{q+} ($q = 3 - 9$) with He and H_2 targets. *J. Phys. At. Mol. Opt. Phys.* **1990**, *23*, L213. [[CrossRef](#)]
10. Reinhold, C.O.; Schultz, D.R.; Olson, R.E.; Kelbch, C.; Koch, R.; Schmidt-Böcking, H. Quantum interference in clothed-ion-atom binary peak structures. *Phys. Rev. Lett.* **1991**, *66*, 1842–1845. [[CrossRef](#)]
11. Wolff, W.; Shinpaugh, J.L.; Wolff, H.E.; Olson, R.E.; Wang, J.; Lencinas, S.; Piscevic, D.; Herrmann, R.; Schmidt-Böcking, H. Diffraction in the binary encounter electron peak observed in collisions of 0.6 MeV amu^{-1} I^{7+} I^{23+} and Au^{11+} projectiles with He and Ar. *J. Phys. B At. Mol. Phys.* **1992**, *25*, 3683–3691. [[CrossRef](#)]
12. Shinpaugh, J.L.; Wolff, W.; Wolf, H.E.; Ramm, U.; Jagutzki, O.; Schmidt-Böcking, H.; Wang, J.; Olson, R.E. Transition from quantum to quasi-classical behaviour of the binary encounter peak in collisions of 0.6 to 3.6 MeV amu^{-1} I^{23+} and Xe^{21+} with He and Ar. *J. Phys. B At. Mol. Phys.* **1993**, *26*, 2869–2878. [[CrossRef](#)]
13. Monti, J.M.; Rivarola, R.D.; Fainstein, P.D. FAST TRACK COMMUNICATION: Quantum interferences in swift highly-charged dressed-ion atom collisions. *J. Phys. B At. Mol. Phys.* **2008**, *41*, 201001. [[CrossRef](#)]
14. Monti, J.M.; Rivarola, R.D.; Fainstein, P.D. Distorted wave theories for dressed-ion-atom collisions with GSZ projectile potentials. *J. Phys. B At. Mol. Phys.* **2011**, *44*, 195206. [[CrossRef](#)]
15. Esponda, N.J.; Quinto, M.A.; Rivarola, R.D.; Monti, J.M. Dynamic screening and two-center effects in neutral and partially dressed ion-atom collisions. *Phys. Rev. A* **2022**, *105*, 032817. [[CrossRef](#)]
16. Madesis, I.; Dimitriou, A.; Laoutaris, A.; Lagoyannis, A.; Axiotis, M.; Mertzimekis, T.; Andrianis, M.; Harissopoulos, S.; Benis, E.P.; Sulik, B.; et al. Atomic Physics with Accelerators: Projectile Electron Spectroscopy (APAPES). *J. Phys. Conf. Ser.* **2015**, *583*, 012014. [[CrossRef](#)]
17. Madesis, I.; Laoutaris, A.; Zouros, T.J.M.; Nanos, S.; Benis, E.P. Projectile electron spectroscopy and new answers to old questions: Latest results at the new atomic physics beamline in Demokritos, Athens. In *State-of-the-Art Reviews on Energetic Ion-Atom and Ion-Molecule Collisions*; Belkić, D., Bray, I., Kadyrov, A., Eds.; World Scientific: Singapore, 2019; Volume 2, Chapter 1, pp. 1–31. [[CrossRef](#)]
18. Madesis, I.; Laoutaris, A.; Nanos, S.; Passalidis, S.; Dubois, A.; Zouros, T.J.M.; Benis, E.P. State-resolved differential cross sections of single electron capture in swift collisions of C^{4+} ($1s2s\ ^3S$) ions with gas targets. *Phys. Rev. A* **2022**, *105*, 062810. [[CrossRef](#)]
19. Zouros, T.J.M.; Benis, E.P. The hemispherical deflector analyser revisited. I. motion in the ideal $1/r$ potential, generalized entry conditions, Kepler orbits and spectrometer basic equation. *J. Electron Spectrosc. Relat. Phenom.* **2002**, *125*, 221. [[CrossRef](#)]
20. Benis, E.P.; Zouros, T.J.M. The hemispherical deflector analyser revisited. II. Electron-optical properties. *J. Electron Spectrosc. Relat. Phenom.* **2008**, *163*, 28–39. [[CrossRef](#)]
21. Harissopoulos, S.; Andrianis, M.; Axiotis, M.; Lagoyannis, A.; Karydas, A.G.; Kotsina, Z.; Laoutaris, A.; Apostolopoulos, G.; Theodorou, A.; Zouros, T.J.M.; et al. The Tandem Accelerator Laboratory of NCSR Demokritos: Current status and perspectives. *Eur. Phys. J. Plus* **2021**, *136*, 617. [[CrossRef](#)]
22. Zouros, T.J.M.; Lee, D.H., Zero Degree Auger Electron Spectroscopy of Projectile Ions. In *Accelerator-Based Atomic Physics: Techniques and Applications*; Shafroth, S.M., Austin, J.C., Eds.; AIP: Woodbury, NY, USA, 1997; Volume 13, pp. 426–479.
23. Nanos, S.; Quinto, M.A.; Madesis, I.; Laoutaris, A.; Zouros, T.J.M.; Rivarola, R.D.; Monti, J.M.; Benis, E.P. Subshell contributions to electron capture into the continuum in MeV/u collisions of deuterons with multielectron targets. *Phys. Rev. A* **2022**, *105*, 022806. [[CrossRef](#)]
24. Toburen, L.H.; Dubois, R.D.; Reinhold, C.O.; Schultz, D.R.; Olson, R.E. Experimental and theoretical study of the electron spectra in 66.7–350-keV/u $C^+ + He$ collisions. *Phys. Rev. A* **1990**, *42*, 5338–5347. [[CrossRef](#)] [[PubMed](#)]
25. Fregenal, D.; Monti, J.M.; Fiol, J.; Fainstein, P.D.; Rivarola, R.D.; Bernardi, G.; Suárez, S. Experimental and theoretical results on electron emission in collisions between He targets and dressed Li^{q+} ($q = 1, 2$) projectiles. *J. Phys. B At. Mol. Phys.* **2014**, *47*, 155204.
26. Hillenbrand, P.M.; Hagmann, S.; Monti, J.M.; Rivarola, R.D.; Blumenhagen, K.H.; Brandau, C.; Chen, W.; DuBois, R.D.; Gumberidze, A.; Guo, D.L.; et al. Strong asymmetry of the electron-loss-to-continuum cusp of multielectron U^{28+} projectiles in near-relativistic collisions with gaseous targets. *Phys. Rev. A* **2016**, *93*, 042709. [[CrossRef](#)]
27. Green, A.E.; Sellin, D.L.; Zachor, A.S. Analytic Independent-Particle Model for Atoms. *Phys. Rev.* **1969**, *184*, 1–9. [[CrossRef](#)]
28. Szydlik, P.P.; Green, A.E. Independent-particle-model potentials for ions and neutral atoms with $Z \leq 18$. *Phys. Rev.* **1974**, *9*, 1885–1894. [[CrossRef](#)]
29. Garvey, R.H.; Jackman, C.H.; Green, A.E.S. Independent-particle-model potentials for atoms and ions with $36 < Z \leq 54$ and a modified Thomas–Fermi atomic energy formula. *Phys. Rev.* **1975**, *12*, 1144–1152. [[CrossRef](#)]

30. Belkić, D. A quantum theory of ionisation in fast collisions between ions and atomic systems. *J. Phys. B At. Mol. Phys. At. Mol. Phys.* **1978**, *11*, 3529–3552. [[CrossRef](#)]
31. Clementi, E.; Roetti, C. Roothaan-Hartree-Fock atomic wavefunctions: Basis functions and their coefficients for ground and certain excited states of neutral and ionized atoms, $Z \leq 54$. *At. Data Nucl. Data Tables* **1974**, *14*, 177. [[CrossRef](#)]
32. Gulyás, L.; Egri, S.; Ghavaminia, H.; Igarashi, A. Single and multiple electron removal and fragmentation in collisions of protons with water molecules. *Phys. Rev. A* **2016**, *93*, 032704. [[CrossRef](#)]
33. Brauner, M.; Macek, J.H. Ion-impact ionization of He targets. *Phys. Rev. A* **1992**, *46*, 2519–2531. [[CrossRef](#)]
34. Monti, J.M.; Quinto, M.A.; Rivarola, R.D. A Complete CDW theory for the single ionization of multielectronic atoms by bare ion impact. *Atoms* **2021**, *9*, 3. [[CrossRef](#)]
35. Belkić, D.; Gayet, R.; Salin, A. Electron capture in high-energy ion-atom collisions. *Phys. Rep.* **1979**, *56*, 279–369. [[CrossRef](#)]
36. Leclerc, J.C. Configuration interaction study of H₂ using a modified Slater-type orbital. *Chem. Phys. Lett.* **1974**, *28*, 546–547. . [[CrossRef](#)]
37. Laoutaris, A.; Nanos, S.; Madesis, I.; Passalidis, S.; Benis, E.P.; Dubois, A.; Zouros, T.J.M. Coherent treatment of transfer-excitation processes in swift ion-atom collisions. *Phys. Rev. A* **2022**, *106*, 022810. [[CrossRef](#)]
38. Lee, D.H.; Zouros, T.J.M.; Sanders, J.M.; Richard, P.; Anthony, J.M.; Wang, Y.D.; McGuire, J.H. K-shell Ionization of O⁴⁺ and C²⁺ ions in fast collisions with H₂ and He gas targets. *Phys. Rev. A* **1992**, *46*, 1374–1387. . [[CrossRef](#)] [[PubMed](#)]

Disclaimer/Publisher's Note: The statements, opinions and data contained in all publications are solely those of the individual author(s) and contributor(s) and not of MDPI and/or the editor(s). MDPI and/or the editor(s) disclaim responsibility for any injury to people or property resulting from any ideas, methods, instructions or products referred to in the content.